Neural networks for FDTD-backed permittivity reconstruction

Vadim V. Yakovlev
Department of Mathematical Sciences, Worcester Polytechnic Institute, Worcester, Massachusetts, USA
Ethan K. Murphy
Department of Mathematics, Colorado State University, Colorado, USA
E. Eugene Eves
The Ferrite Company, Inc., Hudson, New Hampshire, USA

Received August 2004

Abstract

Purpose – To outline different versions of a novel method for accurate and efficient determining the dielectric properties of arbitrarily shaped materials.

Design/methodology/approach – Complex permittivity is found using an artificial neural network procedure designed to control a 3D FDTD computation of *S*-parameters and to process their measurements. Network architectures are based on multilayer perceptron and radial basis function nets. The one-port solution deals with the simulated and measured frequency responses of the reflection coefficient while the two-port approach exploits the real and imaginary parts of the reflection and transmission coefficients at the frequency of interest.

Findings – High accuracy of permittivity reconstruction is demonstrated by numerical and experimental testing for dielectric samples of different configuration.

Research limitations/implications – Dielectric constant and the loss factor of the studied material should be within the ranges of corresponding parameters associated with the database used for the network training. The computer model must be highly adequate to the employed experimental fixture.

Practical implications – The method is cavity-independent and applicable to the sample/fixture of arbitrary configuration provided that the geometry is adequately represented in the model. The two-port version is capable of handling frequency-dependent media parameters. For materials which can take some predefined form computational cost of the method is very insignificant.

Originality/value – A full-wave 3D FDTD modeling tool and the controlling neural network procedure involved in the proposed approach allow for much flexibility in practical implementation of the method.

Keywords Numerical analysis, Neural nets, Dielectric properties

Paper type Technical Paper

1. Introduction

Recently, microwave power engineers have taken a particular interest in complex permittivity, $\varepsilon = \varepsilon' - i\varepsilon''$. While modern electromagnetic simulators allow the engineers to extensively characterize a constructed device prior to making a physical prototype, in order to perform a trustworthy simulation, it is necessary to have reliable knowledge of the dielectric properties of the materials being modeled.

COMPEL: The International Journal for Computation and Mathematics in Electrical and Electronic Engineering
Vol. 24 No. 1, 2005
pp. 291-304

0332-1649
DOI 10.1108/03321640510571318

Determination of dielectric constant ε' and loss factor ε'' of practical materials is a difficult problem. Perturbation and transmission/reflection techniques and other known methods may give satisfactory results under conditions which are either difficult to follow or simply not acceptable; samples typically require the laborious preparation to comply with strict dimensional tolerance requirements.

With more progress in numerical methods, it has become feasible to develop techniques in which the more difficult tasks are assigned to a simulator while the experimental part is reduced to an elementary measurement. This approach has been taken in the methods using finite element method (FEM) (Deshpande and Reddy, 1995; Coccioli *et al.*, 1999; Thakur and Holmes, 2001) and finite difference time domain (FDTD) (Wäppling-Raaholt and Risman, 2003) and modeling the entire experimental fixtures. To further explore this trend, the present paper outlines the principal aspects of a novel efficient technology for permittivity reconstruction.

In our previous work (Eves *et al.*, 2004), we have proposed an approach involving an experimental setup (a closed cavity with an embedded measured sample), whose *S*-parameters are computed by the FDTD method and measured by a network analyzer. Dielectric constant and the loss factor are determined in the course of processing of simulated and measured data by an optimization procedure based on artificial neural networks (ANN).

In the present contribution, we generalize the capabilities of this method by considering other network architectures built on the multilayer perceptron (MLP) and the radial basis function (RBF) ANN, checking different options in network training, and expanding the class of suitable materials to the ones with frequency-dependent media parameters. Since the underlying modeling technique easily handles arbitrary sample/fixture geometry and ANN technology is capable of generalizing the processed data and adjusting to the physical characteristics of the cavity, our method is presented as a flexible and efficient technique of permittivity reconstruction well suited to practical applications.

2. Method of permittivity reconstruction

2.1 Network architectures

We consider two basic one-hidden-layer architectures associated with two types of the experimental setups – a one-port structure intended for measurement of the reflection coefficient S_{11} and a two-port system, which also quantifies the transmission coefficient S_{21}. The configurations of the closed systems considered in our analysis are shown in Figure 1 while the corresponding networks are shown in Figures 2 and 3.

For network training and testing, we use information generated in the modeling phase of the method; the latter is powered by the 3D FDTD method. In the first approach, the network input receives the simulated values of $|S_{11}|$ at n points of the interval around the frequency of interest f_0 while the network output is associated with ε' and ε''. In the second architecture, the input layers get (and the output layers generate) either the simulated values of $\mathrm{Re}(S_{11})$, $\mathrm{Im}(S_{11})$, $\mathrm{Re}(S_{21})$, $\mathrm{Im}(S_{21})$, or the values of ε' and ε'' for which *S*-parameters are computed at the modeling stage. When the network is well trained, it is supplied with the measured values of *S*-parameters and determines ε' and ε'' of the sample in question.

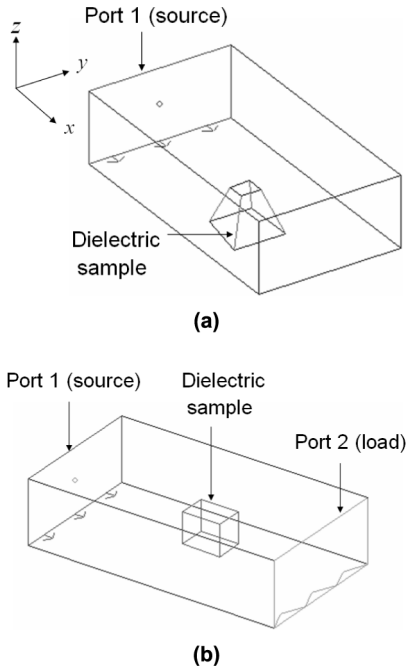

Figure 1.
One- (a) and two-port closed systems (b) with dielectric samples of arbitrary configuration

2.2 One-port solution

In order to describe the computation of complex permittivity with the presented networks, we introduce the vectors $\bar{\mathbf{S}} = [\bar{S}_1 \ldots \bar{S}_n]^{\mathrm{T}} = [|S_{11}|(f_1) \ldots |S_{11}|(f_n)]^{\mathrm{T}}$ and $\boldsymbol{\varepsilon} = [\varepsilon_1 \ \varepsilon_2]^{\mathrm{T}} = [\varepsilon' \ \varepsilon'']^{\mathrm{T}}$. Then the one-port networks generate the following output:

$$\varepsilon_l = \sum_{j=0}^{N} w_{lj}^{3} \sigma \left[\sum_{i=0}^{n} w_{ji}^{2} \bar{S}_i \right], \quad l = 1, 2, \tag{1}$$

where $\sigma(\cdot) = \tanh(\cdot)$ is the activation function used for the hidden neurons, and $w_{pq}^{2|3}$ represents the network weights of the links between the qth neuron in the first or second layer and the pth neuron in the second or third layer; the activation function for the output neurons is a linear function. In the $2 \times n$-input network, $N = N_A$ and $N = N_B$ for Net A and Net B, respectively.

The training data are pairs of $(\bar{\mathbf{S}}_k, E_k)$, $k = 1, \ldots, P$, where E_k is the desired outputs of the network with input $\bar{\mathbf{S}}_k$ (i.e. the values of dielectric constant and the loss factor for which $\bar{\mathbf{S}}_k$ have been simulated), and P is the number of training vectors. The aim is to adjust the vector of network weights $\mathbf{w}$ in order to reduce the errors defined as:

$$e_{\varepsilon_l} = \frac{1}{2} \sum_{k=1}^{P} |\varepsilon_l(\bar{\mathbf{S}}_k, \mathbf{w}) - E_k|^2 \tag{2}$$

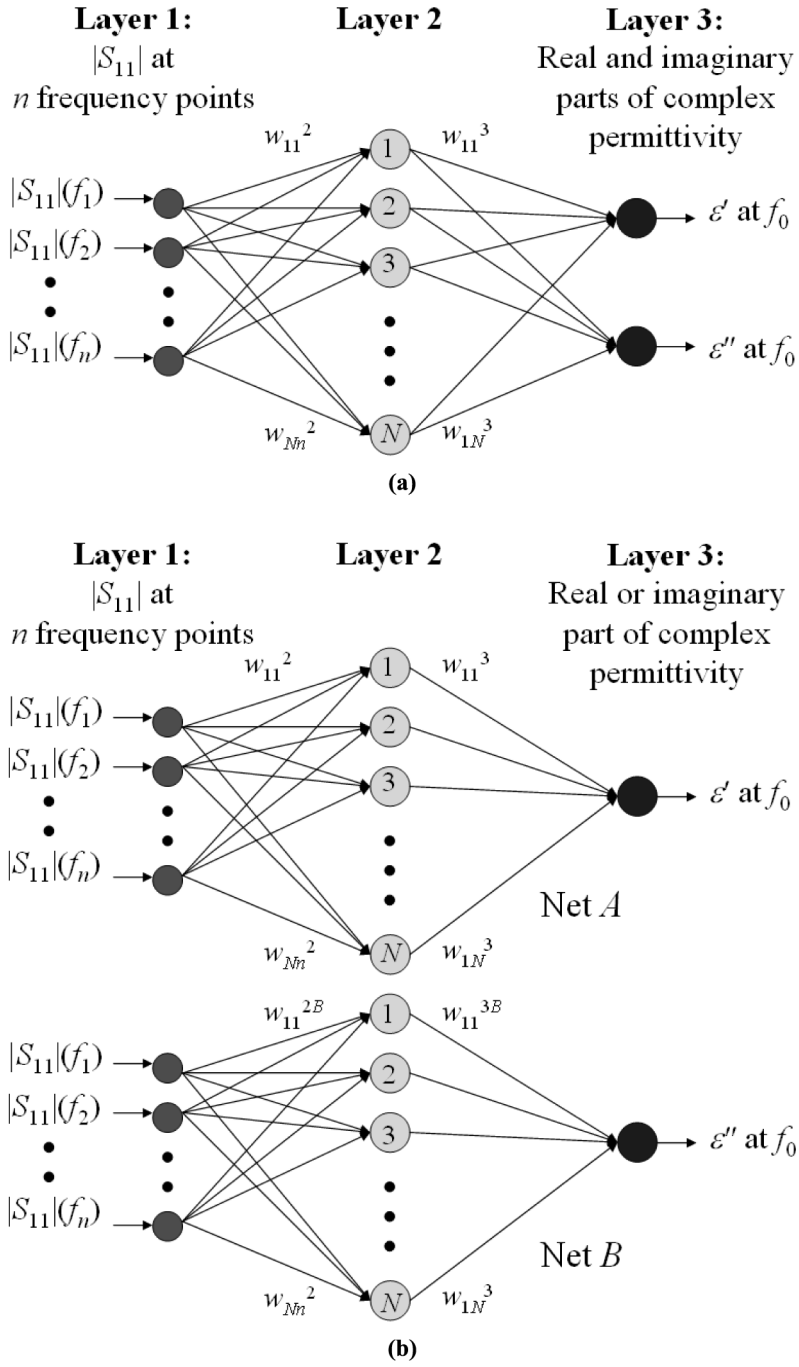

Figure 2.
MLP networks for the one-port system: (a) n- and (b) $2 \times n$-input architectures

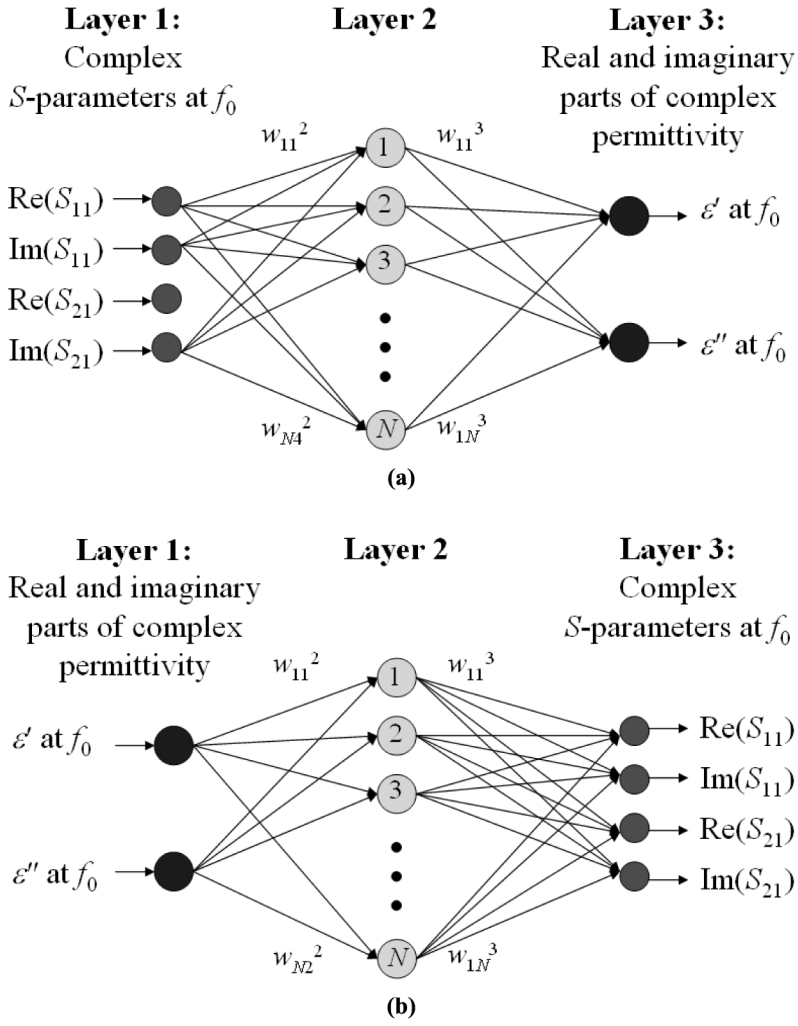

Figure 3.
MLP and RBF networks for the two-port structure: (a) 4- and (b) 2-input architectures

where $\varepsilon_l(\bar{\mathbf{S}}_k, \mathbf{w})$ is the ANN output for input $\bar{\mathbf{S}}_k$. The errors depend on the way the network is trained as well as on its configuration, i.e. on the number of hidden neurons. To minimize the errors (and improve the quality of learning), we determine this number by a standard trial-and-error process applied to the same training data set.

Two training algorithms, namely, back propagation technique and the second-order gradient-based technique are implemented with the use of the gradient method (iterations from 1 to 200) and the Levenberg-Marquardt method (iterations beyond 200), respectively.

Since the one-port approach deals with the frequencies different from f_0, we have a fundamental restriction on the accuracy of this version of the method applied to the materials with frequency-dependent media parameters. FDTD computation of a frequency response is performed for ε' and ε'' at f_0, and measurement of the reflection coefficient is conducted everywhere in (f_1, f_n); hence the measured values may

correspond only at f_0. This provides motivation for considering alternative network architectures processing the related information only at f_0, and dealing with more parameters representing the system behavior, i.e. with the complex reflection coefficient (S_{11}) and the transmission coefficient (S_{21}).

2.3 Two-port solution

With introduction of the vector $\overline{\overline{\mathbf{S}}} = [\overline{\overline{\mathbf{S}}}_1 \ldots \overline{\overline{\mathbf{S}}}_4]^{\mathrm{T}} = [\mathrm{Re}(S_{11}) \ldots \mathrm{Im}(S_{21})]^{\mathrm{T}}$, the output of the two-port MLP and RBF networks is represented by the formulas

$$\varepsilon_l = \sum_{j=0}^{N} w_{lj}^3 \sigma \left[\sum_{i=0}^{4} w_{ji}^2 \overline{\overline{\mathbf{S}}}_i \right], \quad l = 1, 2, \tag{3}$$

and

$$\overline{\overline{\mathbf{S}}}_l = \sum_{j=0}^{N} w_{lj}^3 \sigma \left[\sum_{i=0}^{2} w_{ji}^2 \varepsilon_i \right], \quad l = 1, \ldots, 4 \tag{4}$$

associated with the 4- and 2-input networks; the hidden neuron activation functions are the hyperbolic tangent and Gaussian function $\sigma(\gamma) = e^{-\gamma^2}$ for MLP and RBF ANN, respectively. A linear activation function is used for the output layer in the networks of both types.

The training data for the 4-input MLP and RBF architectures are pairs of $(\overline{\overline{\mathbf{S}}}_k, E_k)$, and the training error is defined as

$$e_{\varepsilon_l} = \frac{1}{2} \sum_{k=1}^{P} |\varepsilon_l(\overline{\overline{\mathbf{S}}}_k, \mathbf{w}) - E_k|^2 \tag{5}$$

where $\varepsilon_l(\overline{\overline{\mathbf{S}}}_k, \mathbf{w})$ is the ANN output for input $\overline{\overline{\mathbf{S}}}_k$. In the 2-input networks, the training data are pairs of $(\varepsilon_k, \Sigma_k)$, where Σ_k is the desired outputs of the network for inputs ε_k (i.e. the values of *S*-parameters simulated for given ε_k). Computation of error in this case is preceded by minimization of the function:

$$G_k = |\overline{\overline{\mathbf{S}}}_l(\varepsilon_k, \boldsymbol{w}) - \Sigma_k|^2, \quad k = 1, \ldots, P \text{ and } \quad l = 1, \ldots, 4 \tag{6}$$

where $\overline{\overline{\mathbf{S}}}_l(\varepsilon_k, \mathbf{w})$ is the ANN output for input ε_k. The solution to this minimization problem is a set of approximated complex permittivity values. Therefore, the network error is determined from:

$$e_{\overline{\overline{\mathbf{S}}}_l} = \frac{1}{2} \sum_{k=1}^{P} [\mathrm{Min}(G_k) - E_k]^2 \tag{7}$$

For the training, the backpropagation technique and the second-order gradient-based technique are used in the two-port networks just as in the one-port ones.

3. Numerical testing

3.1 One-port structure

All the above ANN algorithms have been implemented in a MATLAB 6 environment. For modeling, we use the full-wave 3D conformal FDTD simulator *QuickWave-3D*

(*QW-3D*) (QuickWave-3D, 1997-2004). Data required for network training are collected by a special procedure that repeatedly runs *QW-3D* to compute *S*-parameters for various values of ε' and ε'' of the sample.

The one-port scheme has been tested numerically for a section of 72×34 mm waveguide with a rectangular ($20 \times 20 \times 30$ mm) dielectric block in the corner near the shorting wall. The FDTD model representing this scenario was built with a nonuniform mesh with 7.5 and 3 mm cubic cells in air and in a dielectric sample, respectively (8,463 cells total).

The networks were trained using vectors of $|S_{11}|$ frequency responses with $n = 3$, $f_1 = 2.4$ GHz, $f_2 = f_0 = 2.45$ GHz, $f_3 = 2.5$ GHz, and with 27 values of complex permittivity from the intervals $5 \leq \varepsilon' \leq 9$ and $0.2 \leq \varepsilon'' \leq 1.0$. The graphs in Figure 4 show the typical sum-squared error produced by the n- and $2 \times n$-input networks for different number of neurons in the second layer. It is seen that for more than ten hidden neurons, the networks are characterized by errors not larger than 10^{-5}.

When tested with the training sets of 51 vectors, the networks demonstrated sufficiently accurate permittivity reconstruction. The desired and actual responses from the $2 \times n$-input MLP are shown in Figure 5: mean square error (MSE) is of order 10^{-3}.

3.2 Two-port structure

The two-port scheme dealing with the *S*-parameters at f_0 has been numerically tested with vectors of $\mathrm{Re}(S_{11})$, $\mathrm{Im}(S_{11})$, $\mathrm{Re}(S_{21})$, and $\mathrm{Im}(S_{21})$ at $f_0 = 915$ MHz for the 497 mm section of a 248×124 mm waveguide containing a rectangular dielectric sample (Table I).

We built the training sets for the values of relative complex permittivity in the ranges $54 \leq \varepsilon' \leq 74$ and $6 \leq \varepsilon'' \leq 30$. The 4- and 2-input MLP and the 4-input RBF ANNs were trained with the sets obtained for 48 equally spaced points in the complex (ε', ε'')-plane and additional points on the border (68 samples total). For the 2-input RBF, where the number of vectors in the training set is equal to the number of hidden neurons, the decision as to how many vectors (i.e. points from the (ε', ε'')-plane) in the database to use was made dynamically. The network was given a small database and the error was computed. The three test points with the greatest error were chosen, and for each point an average was taken between the supposed and the ANN-generated values. This average was then taken for the computation of the next sample for the database. For example, for sample B in position B, the optimal number of training vectors (and hidden neurons) turned out to be 57 (Figure 6). In the 4- and 2-input MLP, N was taken 13 and 14, respectively.

Although all MLP/RBF 4-/2-input networks have demonstrated good performance, some of them were found to be more accurate. In Figure 7, the desired and actual responses are shown for the 2-input RBF network with a corresponding MSE 0.013 while for the 4- and 2-input MLP ANNs, MSEs are 0.029 and 0.073, respectively.

Training sets for the ranges of $36 \leq \varepsilon' \leq 56$ and $4 \leq \varepsilon'' \leq 26$ have also been created. The MLP and RBF networks were trained as described above. The 2-input nets have again shown somewhat lower errors. In Figure 8, typical examples of the desired and actual responses from the MLP networks are presented: in both cases the MSE values are of order 10^{-3}.

The detailed error analysis has been carried out to evaluate the accuracy of the two-port systems with a ± 2 mm divergence in the sample's geometry in each dimension. Numerical experimentation has been performed for $\varepsilon = 57 - i8$ (apple, 88 percent moisture contents), $\varepsilon = 68 - i14$ (cantaloupe, 92 percent), $\varepsilon = 62 - i22$

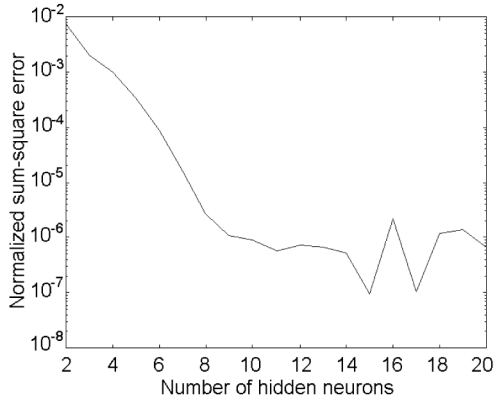

(a)

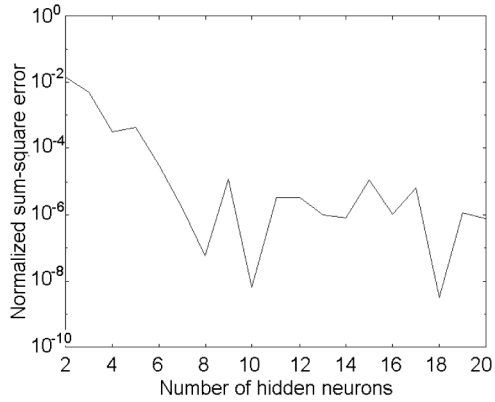

(b)

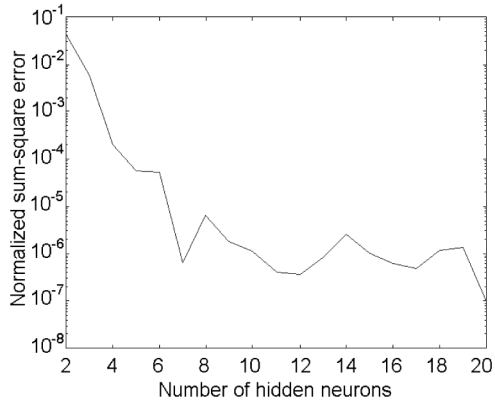

(c)

Figure 4.
Training and testing error of n-input MLP (a) and Net A (b) and Net B (c) of $2 \times n$-input MLP

(potato, 79 percent), and $\varepsilon = 55 - i16$ (sweet potato, 80 percent) (Nelson and Datta, 2001). A typical example of this computation is shown in Figure 9.

Generalizing the results of the analysis conducted for these materials as samples A-D at Positions A-D, we conclude that the 2-input networks can give an error in ε'' less than 5 percent if the sample's geometrical deviation in the longitudinal and transverse directions does not exceed 0.5-1.0 mm. A 10 percent error results from a 1.2-1.5 mm deviation. For ε', the error is less than 5 percent when the deviation is less

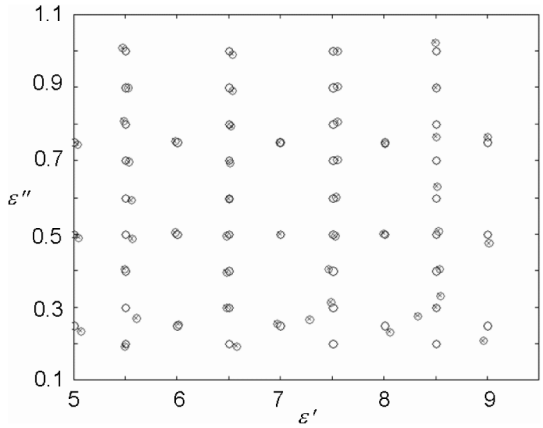

Figure 5.
Complex permittivity reconstructed with the $2 \times n$-input MLP with $N_A = N_B = 10$: circles and crossed circles mark the test data and the actual responses, respectively

Sample	x-, y-, z-dimensions (mm)	Position	Distance (mm) from...
A	$50 \times 50 \times 20$	A	...the second port: 120, ...central line: 0
B	$42 \times 30 \times 50$	B	...the second port: 120, ...central line: 30
C	$20 \times 25 \times 62$	C	...the second port: 120, ...central line: 60
D	$20 \times 25 \times 20$	D	...the second port: 150, ...central line: 30

Table I.
Dielectric samples used in numerical testing of the networks for the two-port scheme

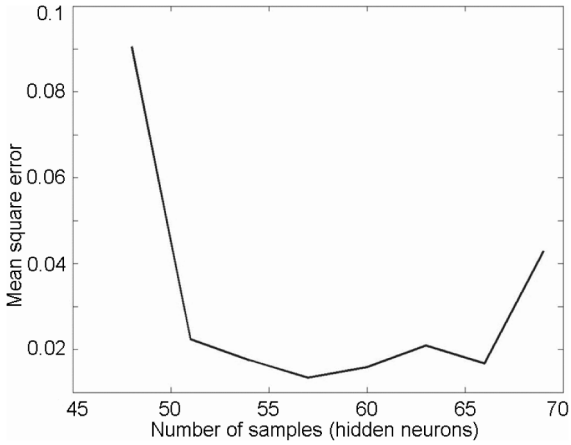

Figure 6.
MSE of the 2-input RBF with the number of training samples from 48 to 69 with step 3

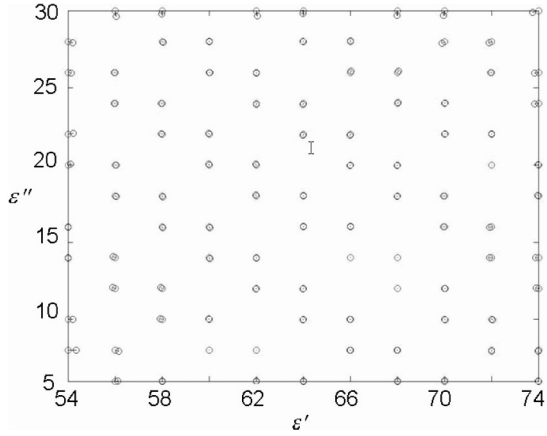

Figure 7.
Complex permittivity of sample B in position B: reconstructed with the 2-input RBF with $N = 57$; the test data and the actual responses

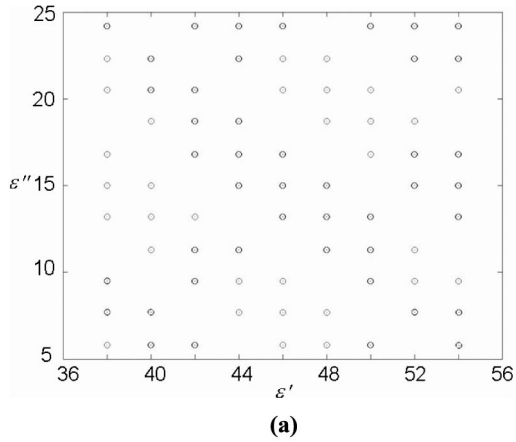

Figure 8.
Complex permittivity of sample C in position B: reconstructed by the 4-input MLP with $N = 13$ (a) and the 2-input MLP with $N = 14$; the test data and the actual responses

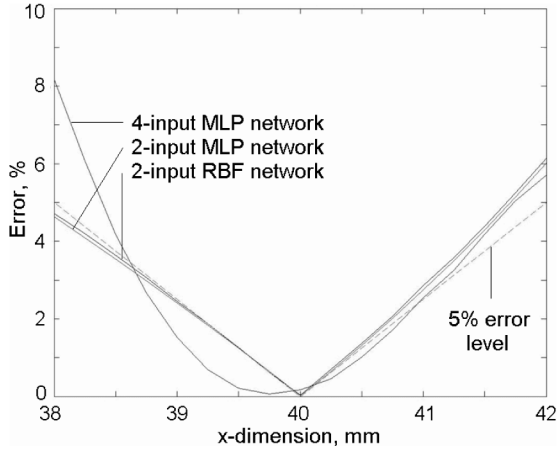

(a)

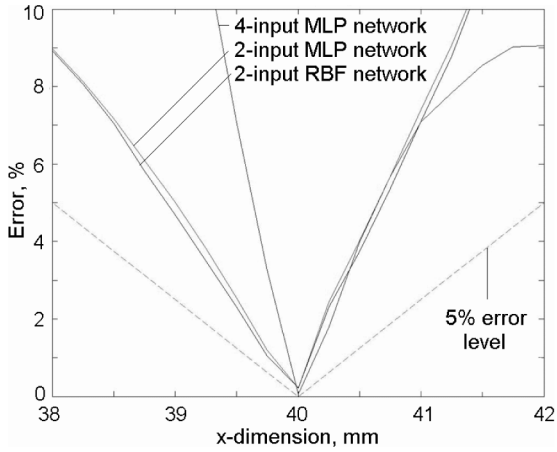

(b)

Figure 9.
Percent error in getting right ε' (a) and ε'' (b) as a function of deviation of training data for the sample dimension in the x-direction: potato as sample B in position B

than 1.2-1.5 mm and always less than 10 percent in the considered 2 mm deviation. Simultaneously, a notable variation of accuracy is observed when the sample's height changes – even if variation in the vertical dimension is quite small. So, for high accuracy, the experimental setup should be constructed to minimize accidental deviations of the sample size in the z-direction.

4. Experimental testing

To show the method in full operation, we have designed the experimental fixture implementing the concept of the one-port solution and thus measuring reflections from a cavity with a dielectric sample (Figure 10). Using a rectangular ($70 \times 70 \times 50$ mm) Teflon block with a cylindrical cutout (radius 25 mm, height 40 mm) suitable for

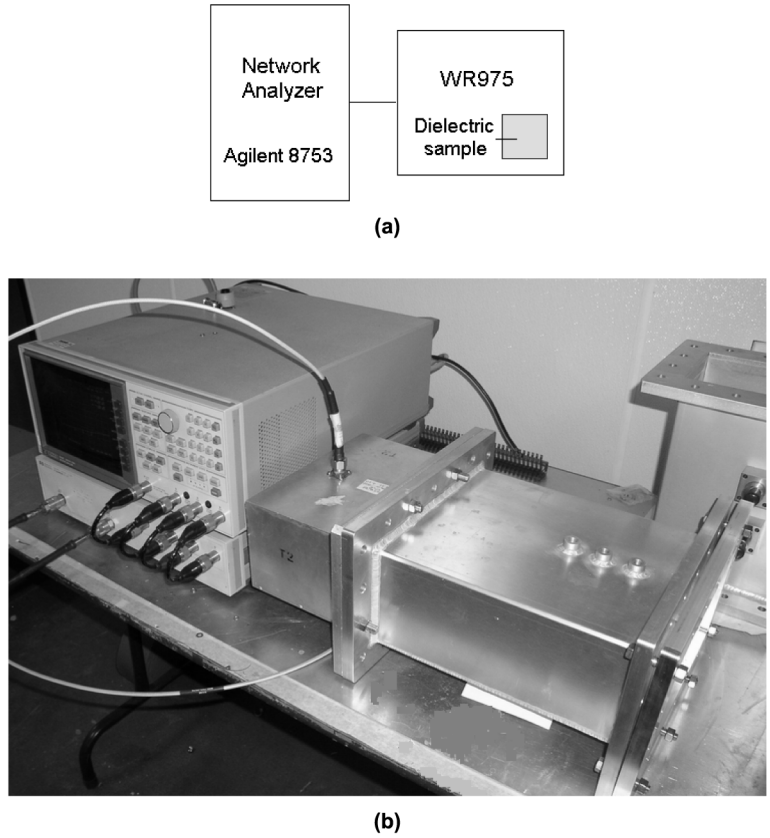

Figure 10.
Diagram (a) and photo (b) of the experimental setup for the one-port solution

holding liquids, we have determined complex permittivity of tap and saline water. The container filled with water was placed on the center line of the waveguide section at 40 mm from the waveguide's shorting wall in the opposite end with respect to the coaxial-waveguide transition.

We used a *QW-3D* model consisting of 71,442 cells with a non-uniform mesh (cell sizes in air, Teflon and water are 15, 5, and 2 mm, respectively) for the entire cavity and dielectric inclusions. The permittivity of Teflon was taken as $2.06 - i0$.

The database of the training and testing sets was created with $n = 3$, $f_1 = 0.91$ GHz, $f_2 = f_0 = 0.915$ GHz, and $f_3 = 0.92$ GHz for $60 \leq \varepsilon' \leq 90$ and $1 \leq \varepsilon'' \leq 20$ and included 108 and 224 vectors, respectively. For the $2 \times n$-input network, the optimal structure was found as having $N_A = 15$ and $N_B = 19$. The normalized sum of squared differences between the desired and actual network responses at the training stage was less than 10^{-4} for both Net A and Net B.

The values of $|S_{11}|$ measured at $f_1 = 0.91$ GHz, $f_2 = 0.915$ GHz, $f_3 = 0.92$ GHz for the Teflon container filled with water were given to the trained network, and it

generated water's dielectric constant and the loss factor. For the sample of known temperature and salinity, ε' and ε'' have been also determined from the model whose average error is 0.3 percent for ε' and 1.8 percent for ε'' (Eves and Yakovlev, 2002). As one can see from Table II, the results are in very close agreement. This confirms the capability of the proposed ANN-based method for accurate reconstructing of complex permittivity of materials.

5. Computer resources

The computational cost of the method is primarily determined by the time required to create a database for network training and testing. The time spent on the training itself is nearly negligible. For example, when working with the two-port scheme and using the 15 and 3.3 mm cells in air and dielectric, respectively, we dealt with the model containing 26,796 cells, and the simulation of one point on a PC with Pentium IV 2.5 GHz processor took 25 s. Hence the database with 149 samples outlined in Section 3 was created within 62 min. Clearly, the accuracy of permittivity reconstruction could be generally improved by increasing the number of samples in the database (and thus, agreeing on a higher computational cost).

Also, the precision of our method may depend on the accuracy of modeling which, in its turn, is conditioned by the FDTD mesh used. In order to virtually exclude an influence of discretization and to make sure that the applied cell sizes for all media involved are adequate, we performed a sensitivity analysis prior to building the databases, subsequently simulating the scenario with slightly smaller cells as long as no substantial change in the results was noticed. All cells' sizes mentioned above are results of this type of an analysis.

6. Conclusion

Our novel technology of permittivity reconstruction which employs FDTD modeling, an ANN-based optimization technique, and elementary measurement of *S*-parameters places minimal physical requirements on fixture and sample geometry and is sufficiently accurate for practical use. Further developments of the method may include its adjustment to non-homogeneous dielectrics and a refinement to allow sample preparation to less strict dimensional tolerances.

The practical advantages of the method are obvious. It does not depend on the associated closed system and thus can be used with any available cavity and any suitable FDTD simulator, not necessarily *QW-3D*. While a relatively large computational effort may be required for creation of a database, the subsequent processes of training and determination of complex permittivity require nearly negligible time. Whenever we work at a fixed frequency with materials that can take

Proposed method	Model (Eves and Yakovlev, 2002)	Divergence (percent)
ε'		
80.6	80.5	0.12
ε''		
4.25	4.30	1.2

Note: Complex permittivity of fresh water with salinity 0.033 percent at temperature 18.6°C determined by the one-port method and the $2 \times n$-input MLP ANN

Table II.

some pre-defined form, the database is created only once. One can do that prior to actual experimental testing, and each new material can be processed thereafter practically in real time – provided that ε' and ε'' of this material are within the ranges specified in the database and that the computer model is based upon the measured experimental fixture.

References

Coccioli, R., Pelosi, G. and Selleri, S. (1999), "Characterization of dielectric materials with the finite-element method", *IEEE Transactions on Microwave Theory and Techniques*, Vol. 47 No. 10, pp. 1106-12.

Deshpande, M.D. and Reddy, C.J. (1995), "Application of FEM to estimate complex permittivity of dielectric material at microwave frequency using waveguide measurements", NASA Contractor Report CR-198203, p. 23.

Eves, E.E. and Yakovlev, V.V. (2002), "Analysis of operational regimes of a high power water load", *Journal of Microwave Power & Electromagnetic Energy*, Vol. 37 No. 3, pp. 127-44.

Eves, E.E., Kopyt, P. and Yakovlev, V.V. (2004), "Determination of complex permittivity with neural networks and FDTD modeling", *Microwave Optical Technology Letters*, Vol. 40 No. 3, pp. 183-8.

Nelson, S. and Datta, A.K. (2001), "Dielectric properties of food materials", in Datta, A.K. and Anantheswaran, R.C. (Eds), *Handbook of Microwave Technology for Food Applications*, Marcel Dekker, Inc., New York, NY, pp. 69-114.

QuickWave-3D (1997-2004), QWED, ul. Zwyciezcow 34/2, 03-938 Warsaw, Poland, www.qwed.com.pl/

Thakur, K.P. and Holmes, W.S. (2001), "An inverse technique to evaluate permittivity of material in a cavity", *IEEE Transactions on Microwave Theory and Techniques*, Vol. 49 No. 10, pp. 1129-32.

Wäppling-Raaholt, B. and Risman, P.O. (2003), "Permittivity determination of inhomogeneous foods by measurement and automated retro-modeling with a degenerate mode cavity", *Proceedings of the 9th Conference on Microwave and HF Heating*, Loughborough, UK, pp. 181-4.